Chemically Driven Hydrodynamic Instabilities

C. Almarcha,[1] P. M. J. Trevelyan,[1] P. Grosfils,[2] and A. De Wit[1]

[1]*Nonlinear Physical Chemistry Unit, CP 231, Faculté des Sciences, Université Libre de Bruxelles (ULB), Campus Plaine, 1050 Brussels, Belgium*

[2]*Microgravity Research Center, Chimie Physique E.P. CP 165/62, Université Libre de Bruxelles (ULB), Av. F.D. Roosevelt 50, 1050 Brussels, Belgium*

(Received 20 April 2009; published 25 January 2010)

In the gravity field, density changes triggered by a kinetic scheme as simple as $A + B \rightarrow C$ can induce or affect buoyancy-driven instabilities at a horizontal interface between two solutions containing initially the scalars A and B. On the basis of a general reaction-diffusion-convection model, we analyze to what extent the reaction can destabilize otherwise buoyantly stable density stratifications. We furthermore show that, even if the underlying nonreactive system is buoyantly unstable, the reaction breaks the symmetry of the developing patterns. This is demonstrated both numerically and experimentally on the specific example of a simple acid-base neutralization reaction.

DOI: 10.1103/PhysRevLett.104.044501 PACS numbers: 82.40.Ck, 47.20.Bp, 47.70.Fw, 82.33.Ln

Convective motion due to hydrodynamic instabilities of an interface between two different fluids are known to impact the spatiotemporal distribution and dynamics of passive scalars in numerous applications. Much less studied is the *active* role that processes involving such scalars can have upon the flow dynamics if these scalars influence a physical property of the fluid such as its density for instance [1–4]. However, coupling between reactive-type processes and hydrodynamics is at the heart of applications in fields as diverse as earth mantle dynamics [5], geological formations [6], supernovae dynamics [7] or CO_2 sequestration [8], to name a few. Often, the specific active role of the scalars on the flow remains difficult to interpret due to difficulties of *in situ* experiments, as well as a lack of quantitative modeling and of simple benchmark experiments on which theories could be tested. In this respect, it is still unclear to what extent reactions involving these scalars can trigger hydrodynamic instabilities in a system that would otherwise remain stable and whether convective structures have the same symmetries in reactive and nonreactive situations.

To gain insight into these issues, let us consider the generic case of a solution containing the scalar A put on top of a solution of B in the gravity field. For nonreactive systems, various hydrodynamic instabilities can impact such a stratification of miscible fluids. The Rayleigh-Taylor instability occurs when the heavier fluid overlies the lighter fluid [9]. If the upper fluid is lighter, the system can also be destabilized either if B diffuses faster than A, because of double-diffusive fingering [10,11], or if a diffusive-layer convection (DLC) instability is triggered when A diffuses faster than B [12]. In all cases, these buoyancy-driven instabilities lead, in nonreactive miscible fluids, to convective motions which develop similarly above and below the initial contact line because of the symmetry of the underlying density gradient [9–12]. The situation can however be very different if a chemical reaction takes place between species A and B upon contact and mixing of the solutions.

We demonstrate indeed both theoretically and experimentally that a reaction as simple as $A + B \rightarrow C$ can strongly impact buoyancy-driven instabilities of a miscible interface between reactive solutions. We show that, not only are chemical reactions able to trigger instabilities in otherwise stable situations, they also break the symmetry of convective structures and instabilities.

To do so, we develop a unifying theoretical reaction-diffusion-convection (RDC) model describing the dynamics inside a porous medium or a vertically orientated Hele-Shaw cell in which a solution of a scalar A at concentration a_0 is placed on top of a solution containing a scalar B at concentration b_0. Species A and B react via the second order mechanism $A + B \rightarrow C$ to produce species C. Typical situations where the reaction destabilizes otherwise stable situations are presented. The resulting patterns are shown to be asymmetric. We next illustrate our general findings experimentally with an acid-base reaction and visualize the dynamics using nonintrusive interferometric and particle image velocimetry (PIV) techniques. Quantitative agreement between experimental results and theoretical predictions is obtained.

We consider a dimensionless RDC model for the concentrations a, b and c of the reactants A, B and product C, respectively, coupled to a Darcy-Brinkman equation for the fluid velocity $\underline{u}$ with $\nabla \cdot \underline{u} = 0$ in the Boussinesq approximation [13]:

$$\nabla p = -\underline{u} + \mathrm{Br}\nabla^2 \underline{u} - \rho(a, b, c)\underline{i}_x, \quad (1a)$$

$$\rho = a + R_b b + R_c c, \quad (1b)$$

$$a_t + \underline{u} \cdot \nabla a = \nabla^2 a - \mathcal{D}ab, \quad (1c)$$

$$b_t + \underline{u} \cdot \nabla b = \delta_b \nabla^2 b - \mathcal{D}ab, \quad (1d)$$

$$c_t + \underline{u} \cdot \nabla c = \delta_c \nabla^2 c + \mathcal{D}ab. \quad (1e)$$

The parameters of the problem are the ratios of the expan-

sion coefficients $(R_b, R_c) = (\frac{\partial\rho}{\partial b}, \frac{\partial\rho}{\partial c})/\frac{\partial\rho}{\partial a}$, and of the diffusion coefficients $(\delta_b, \delta_c) = (D_B, D_C)/D_A$, the initial concentration ratio $\phi = b_0/a_0$, the Damköhler number $\mathcal{D}$ which is the ratio between characteristic hydrodynamic and chemical time scales, and the Brinkman parameter Br quantifying the correction to Darcy's law when the Hele-Shaw cell gap width h is not sufficiently small with regard to the appearing wavelength of the instability [14]. To follow the evolution of the system in time, system (1) is numerically solved using a spectral method [15].

To highlight the role of the reaction in the various possible instability scenarios we focus here first on the situations under which a simple $A + B \rightarrow C$ scheme is able to destabilize a system that would otherwise be stable in its absence. This is the case for equimolar reacting solutions with identical properties ($R_a = R_b$, $\delta_b = 1$), for example. The nonreactive system, with species A and B undergoing purely diffusive mass transfer, is then genuinely stable. However, if the reaction $A + B \rightarrow C$ occurs in the contact zone, a hydrodynamic instability is triggered when the product C has different physical properties.

If the product C diffuses at the same rate as the reactants but is heavier for instance, the reaction yields below the contact line a local Rayleigh-Taylor instability of heavy C on top of light B which induces convection and distorts the initially planar reaction front. In the nonlinear regime [Fig. 1(a)], long narrow fingers then fall downwards from the reaction zone while convection pushes the reaction front upwards. The symmetry around the initial contact zone is broken since the upper stratification of light A on top of heavier C is stable.

The sole effect of differential diffusion can also be isolated by considering a product with a solutal expansion coefficient equal to the sum of the reactants' solutal expansion coefficients. In that case, the density profile is nonconstant only if $\delta_c \neq 1$. Figure 1(b) shows such a situation when $\delta_c < 1$. Two different local instabilities can be observed. As the slower diffusing product C overlies the reactant B, double-diffusive fingering develops between C and B as confirmed by the presence of long narrow fingers falling downwards through the lower solution (like salt fingers [10]). Simultaneously the product C is beneath the faster diffusing reactant A which leads to a DLC instability in the upper part characterized by wider solutal plumes rising upwards. Again, the resulting convection distorts the reaction front and is asymmetric with regard to the initial front position. In both cases of Fig. 1, the chemically induced convection enhances the reaction rate.

To test our instability scenarios in the most general case where $R_a \neq R_b$, $\delta_b \neq 1$, we resort to analyzing the buoyancy-driven instabilities that can be triggered by the neutralization reaction $HCl + NaOH \rightarrow NaCl + H_2O$ with equimolar initial concentrations of the reactants in aqueous solutions. Even though this reaction is exothermic, it can be modeled in porous media or in Hele-Shaw cells by the isothermal system (1) with $A = HCl$, $B = NaOH$ and $C = NaCl$. Indeed, as heat diffuses much faster than mass, its contribution to the density gradients is found here to be quantitatively negligible. Typical dimensionless parameters for such a system are $\delta_b \approx 0.61$, $\delta_c \approx 0.50$, $R_b \approx 2.22$, and $R_c \approx 2.17$ [16]. As $\mathcal{D}$ is large for this quasi-instantaneous reaction, the density profile ρ, computed using the large-time asymptotic reaction diffusion concentration profiles [17] through Eq. (1b), provides information on the instability scenario expected [Fig. 2(b)]. For comparison the density profile associated with a nonreactive classical DLC instability is presented in Fig. 2(a). The fast diffusing species A leaves the upper layer faster downwards than species B diffuses upwards. In the absence of a reaction, this diffusivity difference between A and B leads to an antisymmetric density profile with respect to

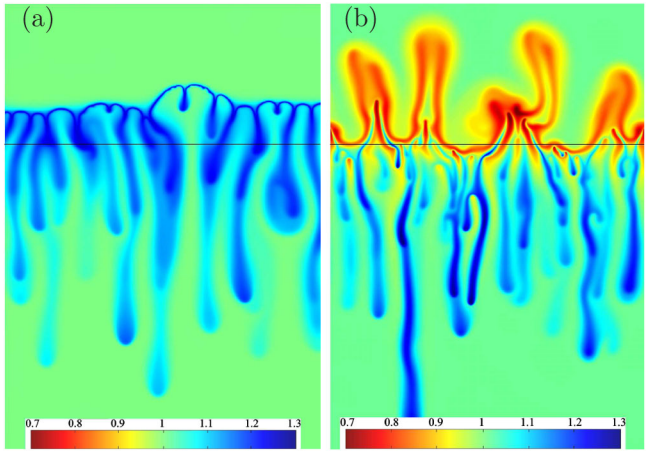

FIG. 1 (color online). 2D density fields obtained by numerically solving (1) using Br = 0, $R_b = \delta_b = \mathcal{D} = \phi = 1$ with (a) $\delta_c = 1$, $R_c = 2.5$, $t = 3.3 \times 10^5$ and domain width 1.9×10^4; (b) $\delta_c = 0.5$, $R_c = 2$, $t = 10^5$ and domain width 8.2×10^3. The black line corresponds to the initial contact line.

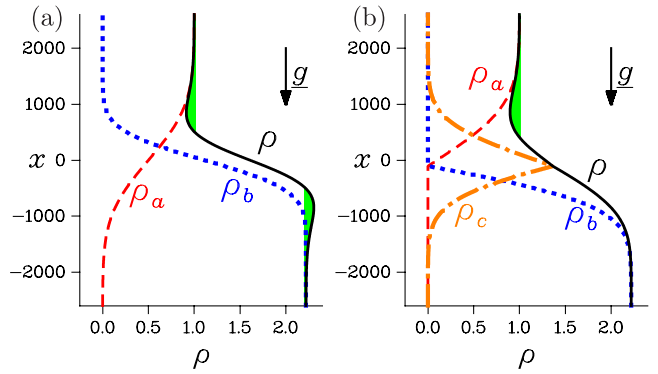

FIG. 2 (color online). Total dimensionless density profile $\rho(x) = \rho_a + \rho_b + \rho_c$ at $t = 3 \times 10^5$ where ρ_ξ corresponds to the density contribution from species ξ. (a) Nonreactive case ($\mathcal{D} = 0$, $\delta_b = 0.3$, $R_b = 2.22$). (b) Reactive case with experimental values. Shaded zones show the sources of instability, i.e., with unstable density stratifications.

the initial contact line $x = 0$ with depletion of the fast diffusing species on top and accumulation of it in the lower part. The resulting nonmonotonic density profile yields two distinct zones of convective motion [shaded zones on Fig. 2(a)] that develop at symmetric distances from $x = 0$ in the nonreactive DLC. Figure 2(b) reports the corresponding density profile for the acid-base system with equimolar initial concentrations. The reactive system behaves differently as the reactants cannot coexist outside of the reaction zone and the density profile is asymmetric [Fig. 2(b)]. The only locally unstable density stratification is in the upper solution, where the resulting convection remains confined by a stabilizing monotonically increasing density in the basic solution.

In order to confirm this theoretical prediction, we use an experimental setup consisting of a vertically oriented Hele-Shaw cell made of two glass plates 3.1 cm wide and 5 cm high separated by a gap width of either 0.5 or 1 mm. The initial condition consists of an aqueous HCl solution placed on top of an equimolar aqueous NaOH solution in the absence of any color indicator (Fig. 3) and obtained using a specific device developed for the study of interfacial instabilities [18]. The visualization of the concentration patterns is obtained by digital interferometry based on a Mach-Zehnder type interferometer coupled with a CCD camera. The phase shift $\Delta\Phi(x, y) = 2\pi h\Delta n(x, y)/\lambda$ induced on the light beam ($\lambda = 633$ nm) by the local variation of the refractive index $\Delta n(x, y)$ in the Hele-Shaw cell is computed by a Fourier transform algorithm [19]. The phase image is further corrected by subtracting a reference image in order to eliminate the possible misalignment of the Hele-Shaw cell window with the light beam. Solutions were seeded with neutrally buoyant latex particles of diameter 5 μm to obtain the velocity field by PIV [20], (Fig. 4). Soon after contact, a sinusoidal perturbation grows in the zone slightly above the contact line [Fig. 3(a)]. Later on, fingers develop, merge and grow until they reach the upper limit of the reactor. The convective flow is observed to rise within the fingers and sink between them (Fig. 4). Remarkably, the zone below $x = 0$ remains unperturbed by convection and features only a slow downward diffusive progression of the reaction front in agreement with the theoretically predicted asymmetry of the pattern.

The experimental pattern is numerically reproduced in Fig. 3(b) by integration of the model (1) and reconstruction of the index of refraction n as $n = n_0 + \beta_A a + \beta_B b + \beta_C c$ using the coefficients β_i obtained in [16]. All the characteristics of the experimental dynamics are reproduced. Thus the RDC model (1) provides quantitative agreement with the experiment shown in Fig. 3. We have further investigated the acid-base dynamics quantitatively for various Hele-Shaw cell gap widths (0.5 and 1 mm) and concentrations (0.1, 0.2, 0.5 and 1 M), i.e., varying Br (Fig. 5). As the convection-free base state depends on time, the most amplified wavelength of the perturbations and its instantaneous growth rate slowly evolve in time. We computed these quantities, for both the numerics and the experiments, at the end of the quasilinear regime, i.e., at the time at which the deformations are of the order of the wavelength. Specifically, we extract from the Fourier transform of the velocity map at this time the value of the most unstable wave number and its growth rate given by $\tilde{A}^{-1}d\tilde{A}/dt$ where $\tilde{A}$ is the amplitude of the mode. These values are reported as a function of Br in Fig. 5, showing a good agreement between the numerics and the experiments. The numerical domain width was chosen so that around 50 fingers appear at onset. The general asymptotic dependence on the parameter Br is obtained from model (1). In the Darcy limit ($\mathrm{Br} \to 0$) the dimensional wavelength and growth rate scale as $h^{-2}a_0^{-1}$ and $h^4a_0^2$, respectively. In the opposite limit ($\mathrm{Br} \to \infty$), we can neglect $\underline{u}$ in

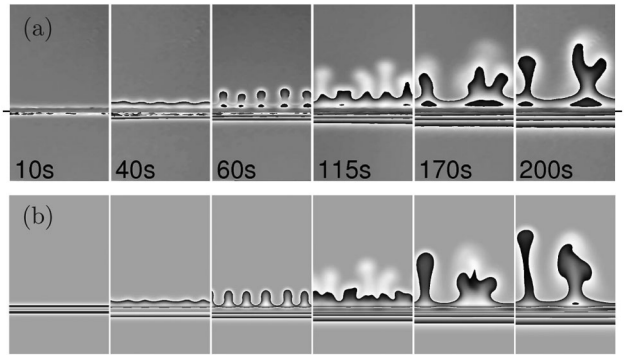

FIG. 3. (a) Interferometry picture of experiments using a 1 M HCl solution on top of a 1 M NaOH solution in a vertical Hele-Shaw cell of gap width 0.5 mm. The initial contact line position is indicated by the black segments at the left and right. The width of the field of view is 13 mm. (b) Corresponding interferometry figure reconstructed at the same times from numerical integration of system (1) for $\phi = \mathcal{D} = 1$, $\delta_b = 0.61$, $\delta_c = 0.5$, $R_b = 2.22$, $R_c = 2.17$ and $\mathrm{Br} = 3.49 \times 10^4$.

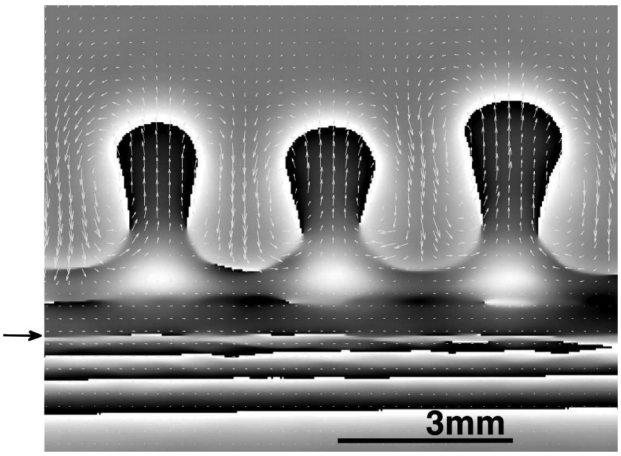

FIG. 4. Superposition of the interferometry figure and velocity map at time 85 s for the fingers of Fig. 3. The black arrow denotes the line of initial contact between solutions. The maximum velocity measured by PIV is 132 μm/s.

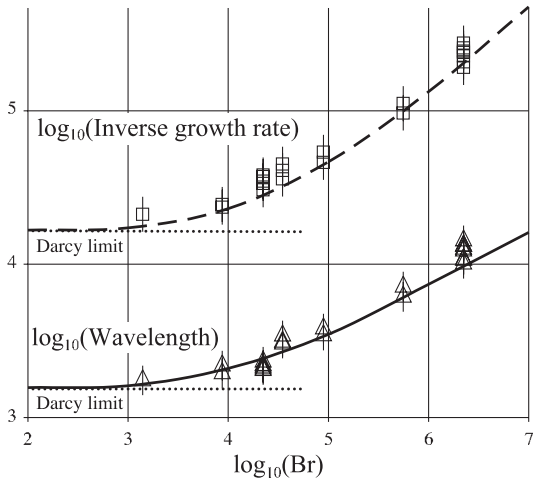

FIG. 5. Experimental nondimensional wavelength (△) and inverse growth rate (□) of the perturbations as a function of Br, and corresponding numerical results shown by the solid and dashed lines, respectively. The porous media limit (Darcy limit) is recovered for Br → 0 (dotted line).

front of $\mathrm{Br}\nabla^2\underline{u}$ in Eq. (1a). When balancing $\mathrm{Br}\nabla^2\underline{u}$ with ρ of order one and seeing from Eq. (1c) that t scales as the length squared, we find that for large Br, the problem is invariant with the length $\sim\mathrm{Br}^{1/3}$ and time $\sim\mathrm{Br}^{2/3}$. These scalings are featured in Fig. 5.

It is important to note that the dynamics presented here are different from those observed in the same acid-base system in the presence of a color indicator [21]. Indeed, in that case, additional convection is obtained in the lower alkaline layer. This shows that the color indicator is actually influencing buoyancy-driven instabilities. A modified version of model (1) including the color indicator is then necessary to reproduce the experimental results in [21]. This also justifies the use of nonintrusive visualization techniques to highlight the phenomena studied here.

In conclusion, we have theoretically and experimentally studied the buoyancy-driven instabilities that can be triggered by an $A + B \rightarrow C$ kinetic scheme when a solution of A lies on top of a solution of B. We have validated a RDC model by quantitative agreement with the dynamics of a HCl/NaOH system in a vertically oriented Hele-Shaw cell. In contradiction to nonreactive systems, the convection triggered by the reaction develops asymmetric patterns with respect to the initial position of the interface.

We are most grateful to K. Eckert for giving us the Hele-Shaw cell [18] and for useful discussions, and to Fr. Dubois for the use of the MRC interferometer. We thank Y. De Decker, A. D'Onofrio, P. Meunier, A. Zalts, and A. Zebib for fruitful discussions and Prodex, FNRS, and ARC-Archimedes for financial support.

[1] D. Avnir and M. Kagan, Nature (London) **307**, 717 (1984).
[2] O. Citri, M. L. Kagan, R. Kosloff, and D. Avnir, Langmuir **6**, 559 (1990).
[3] K. Eckert and A. Grahn, Phys. Rev. Lett. **82**, 4436 (1999).
[4] L. Rongy, P. M. J. Trevelyan, and A. De Wit, Phys. Rev. Lett. **101**, 084503 (2008).
[5] A. Davaille, Nature (London) **402**, 756 (1999).
[6] D. A. Stone and R. E. Goldstein, Proc. Natl. Acad. Sci. U.S.A. **101**, 11 537 (2004).
[7] W. Schmidt, Nature Phys. **2**, 505 (2006).
[8] A. Riaz, M. Hesse, H. A. Tchelepi, and F. M. Orr, Jr., J. Fluid Mech. **548**, 87 (2006).
[9] J. Fernandez, P. Kurowski, P. Petitjeans, and E. Meiburg, J. Fluid Mech. **451**, 239 (2002).
[10] J. S. Turner, *Buoyancy Effects in Fluids* (Cambridge University Press, Cambridge, England, 1979).
[11] S. E. Pringle and R. J. Glass, J. Fluid Mech. **462**, 161 (2002).
[12] A. P. Stamp, G. O. Hughes, R. I. Nokes, and R. W. Griffiths, J. Fluid Mech. **372**, 231 (1998).
[13] Concentrations, speed, length, and time are nondimensionalized by a_0, $u_c = \rho_0 g K \alpha_A a_0/\mu$, $l_c = D_A/u_c$, and $t_c = D_A/u_c^2$, respectively, where D_A and α_A are the diffusion and expansion coefficient of species A, g is the magnitude of the gravitational acceleration, ρ_0 and μ are the density and viscosity of the solvent. K is the permeability, equal to $h^2/12$ for a Hele-Shaw cell with gap width h. The nondimensional density and pressure are defined as $\hat{\rho} = (\rho - \rho_0)/(\rho_A - \rho_0)$ and $\hat{p} = (p - p_0 + \rho_0 g x)K/\mu D_A$, respectively, where ρ_A is the initial density of the solution of A. In (1), hats are dropped. $\mathcal{D} = q a_0 t_c$ where q is the kinetic constant while $\mathrm{Br} = h^2/\pi^2 l_c^2$.
[14] J. Zeng, Y. C. Yortsos, and D. Salin, Phys. Fluids **15**, 3829 (2003).
[15] A. De Wit, Phys. Fluids **16**, 163 (2004).
[16] *CRC Handbook of Chemistry and Physics*, edited by R. C. Weast and M. J. Astle (CRC Press, Boca Raton, FL, 1979), 59th ed.
[17] M. Sinder and J. Pelleg, Phys. Rev. E **62**, 3340 (2000).
[18] Y. Shi and K. Eckert, Chem. Eng. Sci. **63**, 3560 (2008).
[19] M. Takeda, H. Ina, and S. Kobayashi, J. Opt. Soc. Am. **72**, 156 (1982).
[20] P. Meunier and T. Leweke, Exp. Fluids **35**, 408 (2003).
[21] A. Zalts, C. El Hasi, D. Rubio, A. Ureña, and A. D'Onofrio, Phys. Rev. E **77**, 015304(R) (2008).